Supplementary Information

Table of Contents

SI Table 1. Sequences of oligo templates and primers

Name	Sequence
Top Strand Template	5- GCC AGT GAATTC TTA AAATCT CTT ATC AAG AGA GGT GGA GGG ACT GGC CCG ATG AAA CCC GGC AAC CAG CCT TAG GGC ATG GTG CCA ATT CCT GCA -3
Bottom Strand Template	5- AAA GCC ATG GCC GGC CGCTAA AAG AAG AGA CTA CAA GAATCT CTC ATC TTT CAG CGA AAC CGCTGC AGG AATTGG CAC CAT GCC CTA AGG CTG -3
WT Forward Primer	5- TAATAC GACTCA CTATAG AAT CTC TTATCA AGA GAG GTG GAG GG -3
dP0 mutant Forward Primer	5- TAATAC GACTCA CTATAG AAT CTC TTATCC AGA GAG GTG GAG -3
eP0 mutant Forward Primer	5- TAATAC GACTCA CTATAG AAT CTC TGA TCC AGA GAG GTG GAG -3
Aptamer [1] Reverse Primer	5- mAmAT CTC TCA TCT TTC AAC GAA ACC GCT GCA GG -3
AT1 Reverse Primer	5- mAmAG AAG AGA CTA CAA GAATCT CTC ATC TTT CAG CG -3
AT2 Reverse Primer	5- mCmUT CGCTAA AAG AAG AGA CTA CAA GAATCT CTC ATC TTT CAG -3

SI Table 2. Accession number for sequences shown in SI Figure 5.

Genus species strain	Accession
Thermoanaerobacter tengcongensis MB4	NC_003869
Thermoanaerobacter italicus Ab9	NC_013921
Thermoanaerobacter mathranii subsp. mathranii str. A3	NC_014209
Thermoanaerobacterium thermosaccharolyticum DSM 571	NC_014410
Thermoanaerobacter sp. X514	NC_010320
Thermoanaerobacter pseudethanolicus ATCC 33223	NC_010321
Thermoanaerobacter sp. X513	NC_014538
Thermoanaerobacter brockii subsp. finnii Ako-1	NZ_ACQZ01000001
Thermoanaerobacter wiegelii Rt8.81	NZ_ADXD01000015

SI Table 3. Average pairwise difference in P1 helix BPP predicted for *B subtilis* SAM-I riboswitch sequences.

Sequences	*metE/ cysH*	*ykrT/ yxjH*	*ykrW/ metC**	*yxjG/ yxjH**	*yxjG/ ykrT**	*yusC/ cysH**	*yusC/ metE**
Δ_{ave}(total)	0.76	0.24	0.21	0.22	0.20	0.52	0.26
Δ_{ave}(half)	0.88	0.33	0.20	0.40	0.26	0.49	0.40
Δ_{ave}(apt+12)	0.88	0.27	0.22	0.29	0.23	0.58	0.33

BPP was calculated over the range 0-90 °C for transcript lengths beginning with the terminus of the aptamer, as shown in SI Figure 12, the absolute values of the difference in BPP between the specified pairs of sequences was calculated at each temperature/transcript length datapoint. The data points were summed and normalized to compute Δ_{ave}(total). Δ_{ave}(half) is the average calculated using only the second half of the datapoints on the horizontal axis. Δ_{ave}(apt+12) is calculated using only those datapoints for which the transcript length is 13 nucleotides or more longer than the isolated aptamer. Comparison between Δ_{ave}(total), Δ_{ave}(half) and Δ_{ave}(apt+12) indicates that the greatest variability occurs as the transcript is extended beyond the aptamer region for most *B. subtilis* SAM-I riboswitch pairs. Pairwise comparisons have been made only for sequences for which the length of the expression platform chosen was equal to within +/- 1 for each sequence. *Range of transcript length beyond the aptamer differs by 1 nucleotide between the two sequences

Gel mobilities of *metF* SAM-I riboswitch segments

The transcript which is long enough to incorporate an AT2 helix, has the largest relative populations of the slow moving species, both with and without SAM (SI Figure 6, compare lanes for sample E to those for A and B). If the fastest moving band is therefore assumed to represent an OFF state conformer, then gel mobilities indicate that the relative population of the OFF state is much reduced when the transcript extends to include AT2-helix-forming residues. As stated in the main text, introduction of the P0 mutation also reduces the relative intensity of the fastest-migrating band, with or without SAM present (SI Figure 6, lanes C compared to lanes B, and lanes F compared to lanes E). There are a number of possible interpretations for the slowest migrating bands in SI Figure 6. These may correspond to the formation of multimers, or to alternative tertiary folds. For example, the tertiary folding associated with pseudoknot formation may lead to rapid migration[2] in a subset of SAM-bound and unbound molecules, while a subpopulation of unbound molecules remains unfolded.

Supplementary Discussion

Contrasting P1 vs. AT helix competition patterns for the yitJ and metF SAM-I riboswitches

As noted in the main text, the AT1 helix model for the *metF* SAM-I riboswitch is somewhat analogous to the AT helix model generally presented for the yitJ SAM-I riboswitch sequences. In this section we note the differences in sequence and competition topologies between the corresponding P1 and AT helices for the two sequences. We also explore in detail the predicted differences in patterns of predicted BPPs for competing base pairs in this region for the two sequences.

SI Figure 2 illustrates the differences in the competition topologies between the *metF* AT1 and *yitJ* AT helices. While the *metF* AT1 helix presents a one-to-one competition with the P1 helix at each base pair position, the *yitJ* P1 and AT helices each contain exclusive base pairings- the P1 helix has two such base pairs and the AT helix has up to five extra base pairs with a possible U bulge close to the switching region. In the *yitJ* SAM-I riboswitch, the P1 and the AT helices use the same nucleotide sequences to compete for the switching region, and the switching region spans six base pairs. In the *metF* SAM-I riboswitch, the P1 and the AT helices have different base pair compositions (P1: 3 GCs, 7 AUs, 1 GU; AT1: 2GCs, 5 AUs, 3 GUs, 1 UC mismatch). Also the AT helix has the potential to form an additional helical region, overtaking the edge of the P1 helix that is close to the SAM binding pocket, though these additional base pairs will be very unstable in isolation.

The AU base pairs at position 2 and 3 in the P1 helix have been shown to be important in the specific recognition of SAM via electrostatic interaction [3; 4]. In the *yitJ* SAM-I riboswitch AT, the alternative base pair for the U at position 3 is a helix-closing UA base pair in the AT helix, which should not be very stable. In two possible AT models of the *metF* SAM-I riboswitch (SI Figure 1), the corresponding U either forms a UC mispair or unpaired two-residue bulge. Therefore, this U appears to present a point of destabilization of the AT helix which may facilitate nucleation of a P1 helix. Also, in the case of the thermophilic SAM-I riboswitch, it may participate in a switch between alternative AT helices (Figure 1a).

In SI Figure 2c and d the BPPs for all base pairs in the P1 and the AT (or AT1) helix are displayed. The higher the BPP value, the more likely it is for the corresponding base pair to form at that position. If the summation of BPPs for two possible base pairs at one position is 1, an exclusive competition between P1 helix and AT helix base pairing is predicted for the corresponding position. The exclusive competition region (sum > 0.8) in the *yitJ* SAM-I riboswitch (position 3-8) is closer to the SAM binding pocket than that in the *metF* SAM-I riboswitch (position 5-10). The *yitJ* SAM-I riboswitch displays a steady increase in the relative BPP values for AT versus P1 helix formation moving towards the right within the exclusive competition region, while the *metF* SAM-I riboswitch has roughly the same relative BPP values for all positions. Interestingly, a hybrid structure with partial P1 and partial AT helix is observed in the minimal free energy (MFE) structure of the *yitJ* SAM-I riboswitch (SI Figure 2b).

P0 helix—a potential structural element for the ON state conformers

It was not possible to unambiguously obtain evidence for P0 helix formation, even in a mutant which was designed to stabilize the proposed helix. Reduction in SAM binding affinity (Figure 4) and an apparent increase in ON conformer formation (Figure 6) can be explained by a concomitant destabilization of the P1 helix. This interpretation is supported by recovery of binding affinity of SAM to the P0 mutant at low temperature (Figure 4b). Length and therefore stability of the P1 helix is strongly correlated with SAM binding affinity in SAM-I riboswitches[5]. Increased affinity for SAM for the extended WT_AAT_AT1 *metF* SAM-I riboswitch construct as compared to the aptamer (WT_AAT) (Figure 4), can be explained by the introduction of an extra GC base pair in the P1 helix involving a 5'G residue added to aid transcription. Our BPP simulations generally do not predict the P0 helix as a predominant conformer in the wild type version of the *yitJ* SAM-I riboswitch sequences that we have examined, though it is predicted more prominently in *metF* sequences under some circumstances, and with very high probability for the eP0 mutant. On the other hand, if SAM binding were determined solely by the stability of the P1 helix, then displacement of a pyrrolo-C labeled oligonucleotide upon addition of SAM should have been greater upon hybridization with an aptamer construct containing a full length P1 helix than when the hybridization was performed with a similar RNA in which 5' residues were removed to yield a shortened P1 helix. The latter result may be attributed to sequestration of 5' residues in the complete aptamer construct through the formation of a P0 helix.

Caution must be exercised in interpreting SAM binding and RNA folding data for the eP0 mutant, since the nucleotide changes may have additional effects beyond stabilization and destabilization of secondary structure elements. For example, the equivalent residue to A9 in the *yitJ* SAM-I riboswitch X-ray coordinates is involved in an extrahelical dinucleotide stacking interaction. MD simulations indicate that the dinucleotide stack may form and dissociate transiently in both of the crystallized SAM-I riboswitch systems. Since the dinucleotide stacking requires a pseudoknot-stabilized tertiary fold, mutation of A9 may perturb tertiary and possibly secondary structure folding of the riboswitch, as well as SAM binding, if conversion of A to C weakens the dinucleotide stack.

Figure 5a illustrates the fact that conserved stretches of purines are present in three of four junction regions within the aptamer conformation. Since the 5' residues within the P1 helix are pyrimidines, the junction purines offer "decoy" interactions that can compete with P1 helix folding. If, as indicated in Figure 2 and in NMR measurements, magnesium can induce a degree of pseudoknot formation in the absence of SAM, the probability of cross-junction base pairing involving G11 and A12 (D2) would seem less likely than sequestration of G11 and other 5' resides by a P0 (D1) or anti-P4 (D3).

An interesting feature of Figure 5c, where base pairing of residues in J4/1 associated with D3 formation are constrained from forming, is that it seems to predict less heterogeneity in helices P2, P3, and P4 as compared to the unconstrained calculations. Heterogeneity in the P1/AT helix competition region, however, increases, since a significant spread is observed in BPPs for individual base pairs within the respective helices.

Limitations of BPP calculations and the likely impact of pseudoknot formation

The accuracy of BPP calculation is limited by the free energy model and parameters. Current available free energy models should work relatively well for the SAM-I riboswitch because there are fewer non-Watson Crick base pairs as compared to other riboswitches. The software packages which we used in this study utilize the nearest neighbor approximation to caluclate the Free Energy[6]. The BPP results we presented in this study do not take pseudoknot formation into consideration. If the pseudoknot is considered, the BPP of two base pairs sometimes predicted between J1/2 and J3/4 may decrease or may not form. Prediction of pseudoknot formation has recently been incorporated in secondary structure predictions as an additional step [7].

We duplicated a set of simulations for *yitJ* SAM-I riboswitch folding using the alternative RNAStructure package [6] (data not shown). Overall predicted trends were similar to those reported herein, except that ON state conformers predicted a greater contribution from P0 helix formation relative to cross-junction base pairing. Thus, the predicted secondary structure ensembles were predominantly compatible with pseudoknot formation.

Supplementary Methods and Materials

Quantification of structure-probing through base-catalyzed cleavage

Gel images are quantified as described in reference [8; 9]. Briefly, lanes for different samples are defined, bands are aligned to eliminate the distortion due to gel "smiles" and bands are assigned based on Gs in the sequence from T1 digestion and single nucleotide resolution ladder from partial alkaline hydrolysis. Then, the quantification of band intensities is performed using the peak fitting methods implemented in SAFA [9]. The lane in the presence of SAM is normalized to the lane in the absence of SAM, and the data is visualized as a false-color as described in reference[8]. Here the red color indicates increased cleavage in the presence of SAM, the blue color decreased and the white color constant.

Equilibrium Dialysis

The RNA sample was heated at 95 °C for 3 minutes and snap cooled on ice for 5 minutes. Then the RNA was exchanged into 50 mM Tris-HCl (pH 7.5), 25 mM NaMES, 25 mM NaOAc, 100 mM KCl, 2 mM $MgCl_2$ to achieve a specified final concentration. 25 μL of the RNA sample was added to the chamber B of an equilibrium dialysis chamber--DispoDialyzer (Harvard Apparatus), and then the specified concentration of [^{3}H] SAM was added to the chamber A of the dialyzer. The dialyzers were agitated on a nutator for ~8 hours at different temperatures (4 °C & RT/~22°C). Aliquots in the control (no RNA in chamber B) were collected for scintillation counting to confirm that equilibrium had been reached. The ratio of c.p.m of chamber B relative to chamber A, averaged over 3 readings, is reported as a measure of the relative binding affinity. As SAM binding is affected by the conformation of the RNA but also by other factors, it cannot be taken as a quantitative indicator of riboswitch conformation. Therefore we did not quantify binding affinities by Scatchard analysis. We did

acquire data under a series of ligand and RNA concentrations and stoichiometries, in order to optimize sensitivity to affinity changes within differing affinity ranges.

Native gel electrophoresis

The RNA stock was diluted to 50 μM using 10 mM K Phosphate (pH 6.0), 10 mM KCl. The RNA sample was heated at 95 °C for 3 minutes and snap cooled on ice for 5 minutes. The RNA was folded in 1x TB (pH 8.3), 200 mM KCl, 10 mM $MgCl_2$, 20% glycerol with a final concentration of 5 μM and incubated at 37 °C for 1 hour with or without 100 μM SAM. The samples were electrophoresed using 10% native PAGE in 1x TB with 10 mM $MgCl_2$ at 4 °C at 200 V for 16 hours. This type of native gel assay has been used to select the conformation that has response to SAM in ref [10].

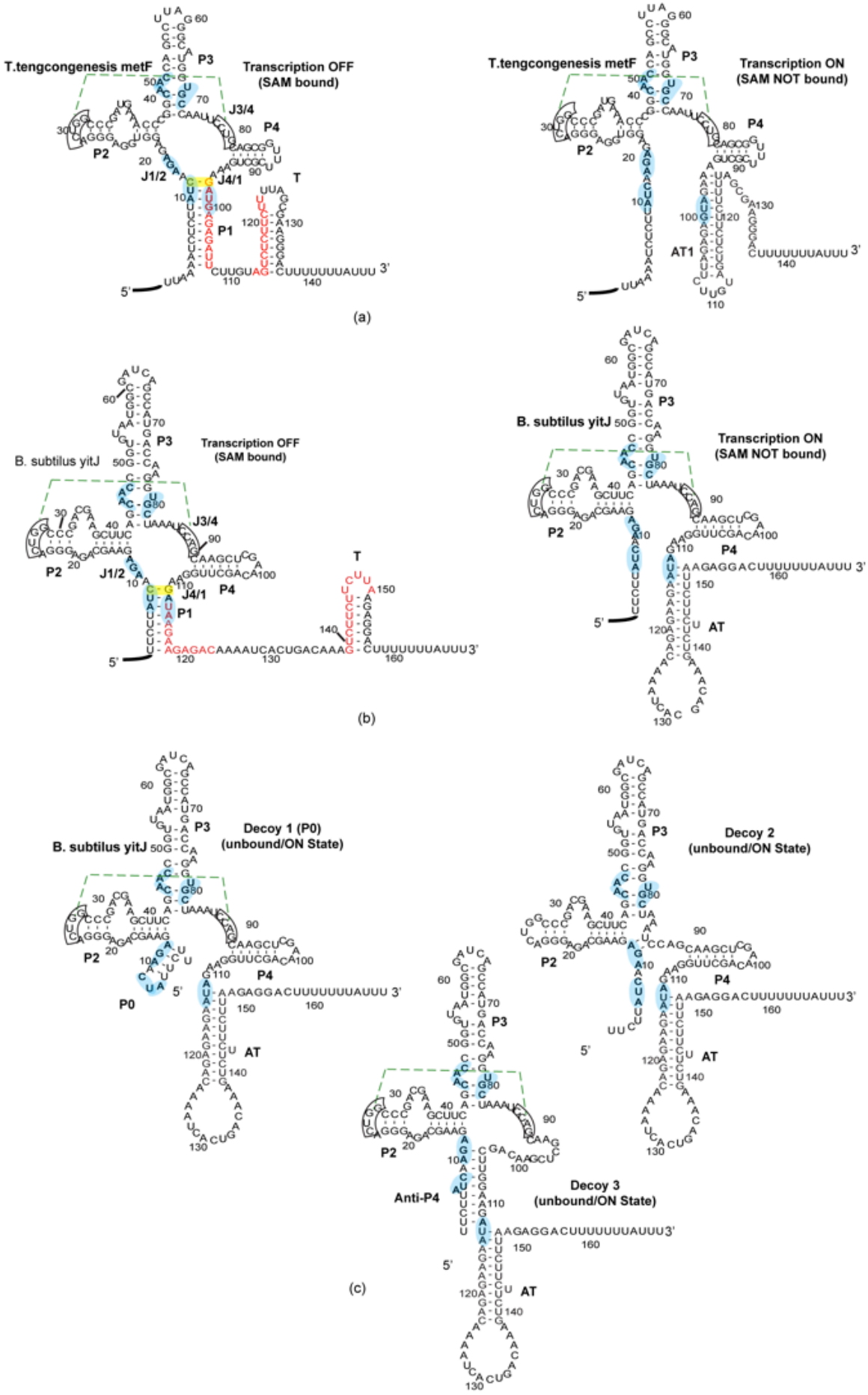
T.tengcongenesis metF
Transcription OFF
(SAM bound)
P3
P2
P4
J3/4
J1/2
J4/1
P1
T
5'
3'
(a)
T.tengcongenesis metF
Transcription ON
(SAM NOT bound)
P3
P2
P4
AT1
5'
3'
B. subtilus yitJ
Transcription OFF
(SAM bound)
P3
P2
J3/4
J1/2
J4/1
P4
P1
T
5'
(b)
B. subtilus yitJ
Transcription ON
(SAM NOT bound)
P3
P2
P4
AT
5'
3'
B. subtilus yitJ
Decoy 1 (P0)
(unbound/ON State)
P3
P2
P4
P0
AT
5'
3'
Decoy 2
(unbound/ON State)
P3
P2
P4
AT
5'
3'
Anti-P4
Decoy 3
(unbound/ON State)
P2
AT
5'
3'
(c)

SI Figure 1. Schematic showing secondary structure transitions in SAM-I riboswitches according proposed models.

(a) Transition between the transcription OFF state (left), favored in the presence of SAM, and the transcription ON state, favored in the absence of SAM for the *B. subtilis yitJ* SAM-I riboswitch.The scheme shown has been proposed by the Breaker[11] and Henkin[12; 13] groups. (b) Schematic of SAM-induced secondary structure switch for the T. tengcongensis metF SAM-I riboswitch as proposed in report of the first X-ray structure[14]. Note that the anti-terminator in this scheme "AT1" differs from that proposed later by Hennelly et al[15] ("AT2") as shown in Figure 1a from the main text. (c) Schematic representation of three "decoy" base pairing interactions predicted by BPP calculations presented in Figure 5 from the main text for the yitJ riboswitch sequence. Note that each interaction sequesters 5' residues, notably G11 from J1/2 and surrounding residues. These alternative secondary structures are therefore not compatible with SAM binding. D1 and D3 also directly block formation of a P1 helix. Residues within five angstroms of SAM according to X-ray coordinates are highlighted in light blue, and residues involved in pseudoknot formation (designated by the dotted green lines) are boxed, as in Figure 1 from the main text. Note that pseudoknot formation is not compatible with D2.

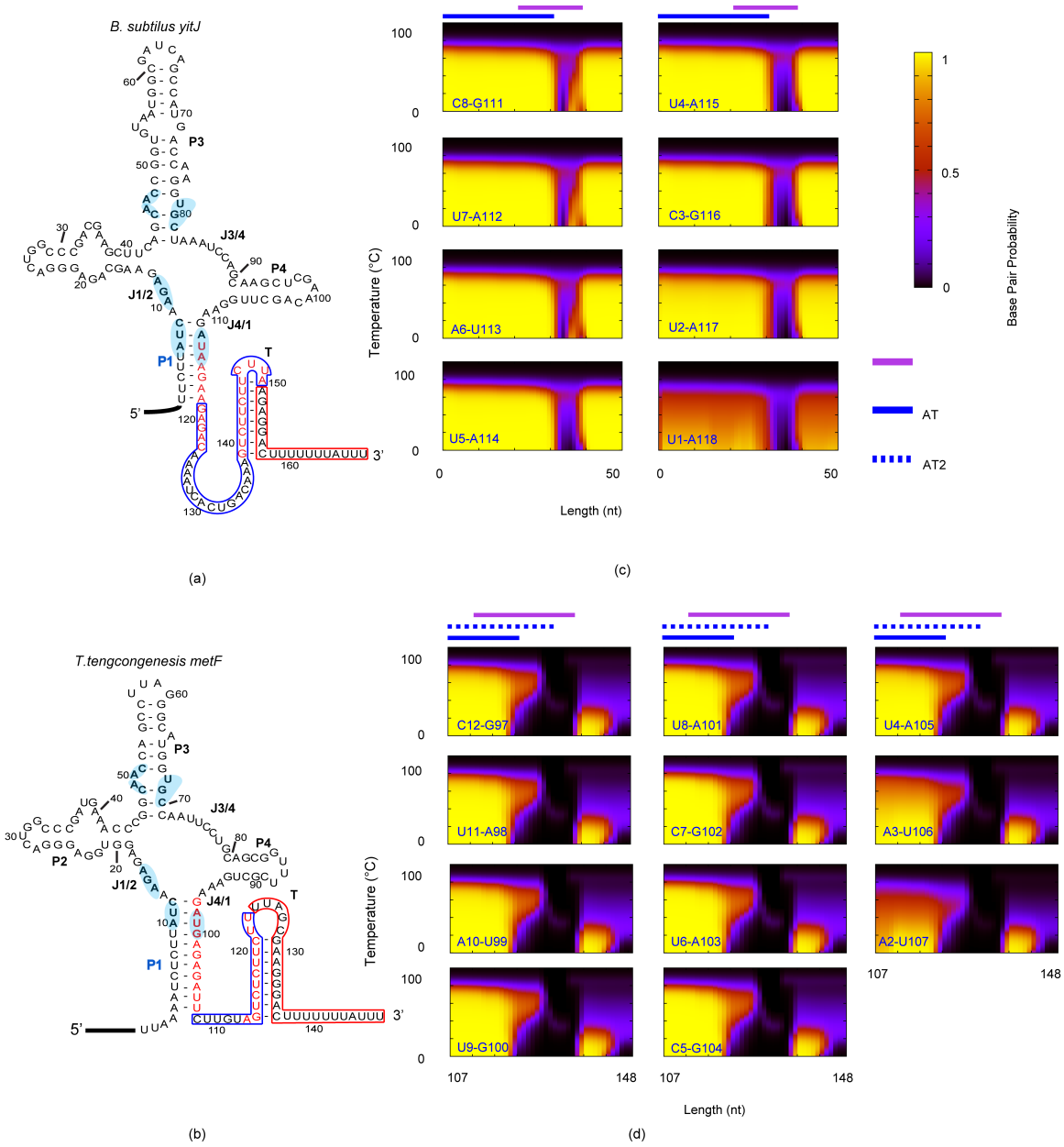

SI Figure 2. BPP of all base pairs in the P1 helix of the yitJ (a, c) and the metF (b, d) SAM-I riboswitches plotted as in Figure 1.

Residues within proximity of SAM according to X-ray coordinates are highlighted as in Figure 1 from the main text.

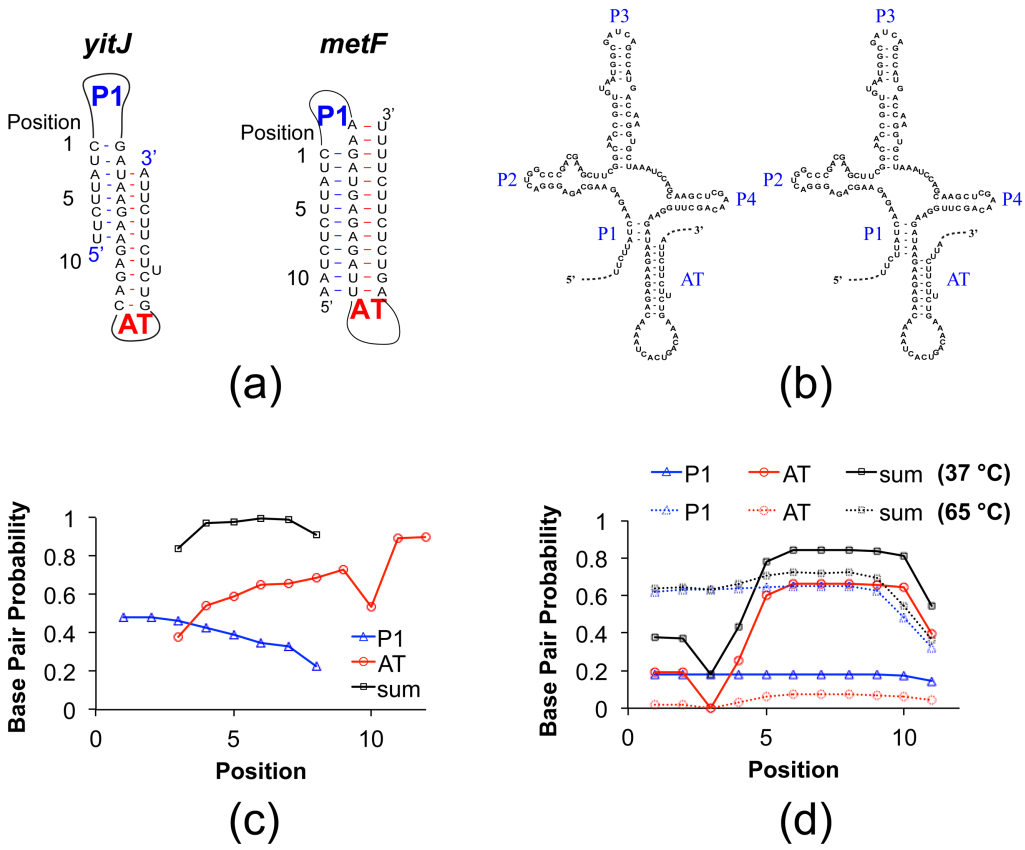

SI Figure 3. Different base pair competition topologies for *yitJ* and *metF* SAM-I riboswitches.

(a) The numbering scheme used to designate each switchable base pair position, as plotted on the horizontal axes. The "sum" is the summation of BPP values for the two possible base pairs each position. (b) Secondary structure representation of possible hybrid intermediate states for the *yitJ* SAM-I riboswitch. The hybrid geometry shown in the left figure is predicted in the MFE structure from RNAfold. (c) BPPs for base pairs involved in formation of P1 or AT helix at 37 °C for the *B.subtilis yitJ* SAM-I riboswitch. (d) BPPs for base pairs involved in formation of P1 or AT helix at 37 °C and 65 °C for *T.tengcongenesis metF* SAM-I riboswitch. Note that for the *yitJ* SAM-I riboswitch, positions one and two can only form P1helix pairs, while only AT pairs can form for positions 9-13.

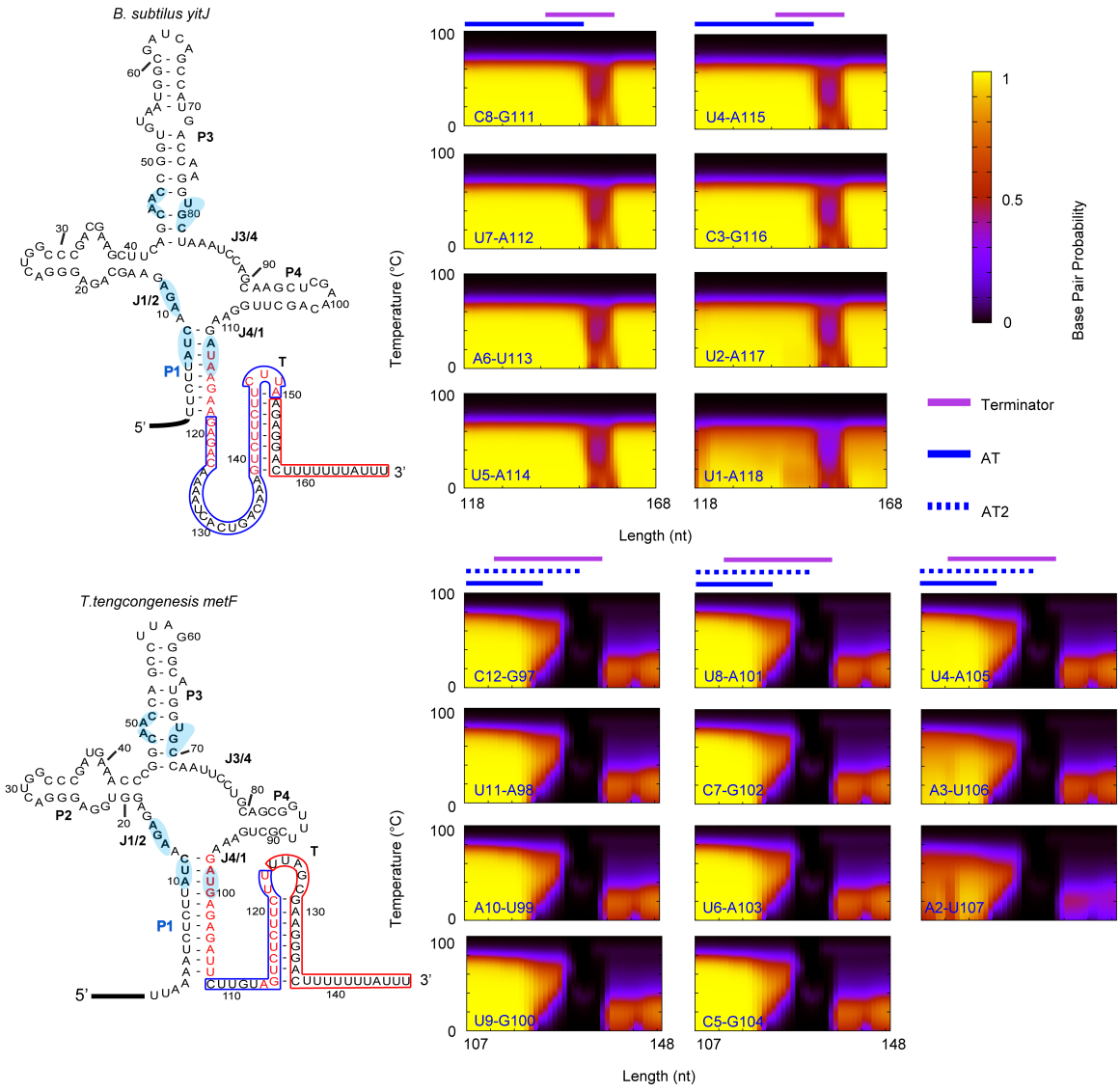

SI Figure 4. Similar plot as SI Figure 2 but BPP calculations were performed with the sequence starting at the transcription start site, rather than at the 5' end of the aptamer sequence.

(a) for the *B. subtilis yitJ* SAM-I riboswitch sequence and (b) for the *T. tengcongensis metF* sequence. Residues within proximity of SAM according to X-ray coordinates are highlighted as in Figure 1 from the main text.

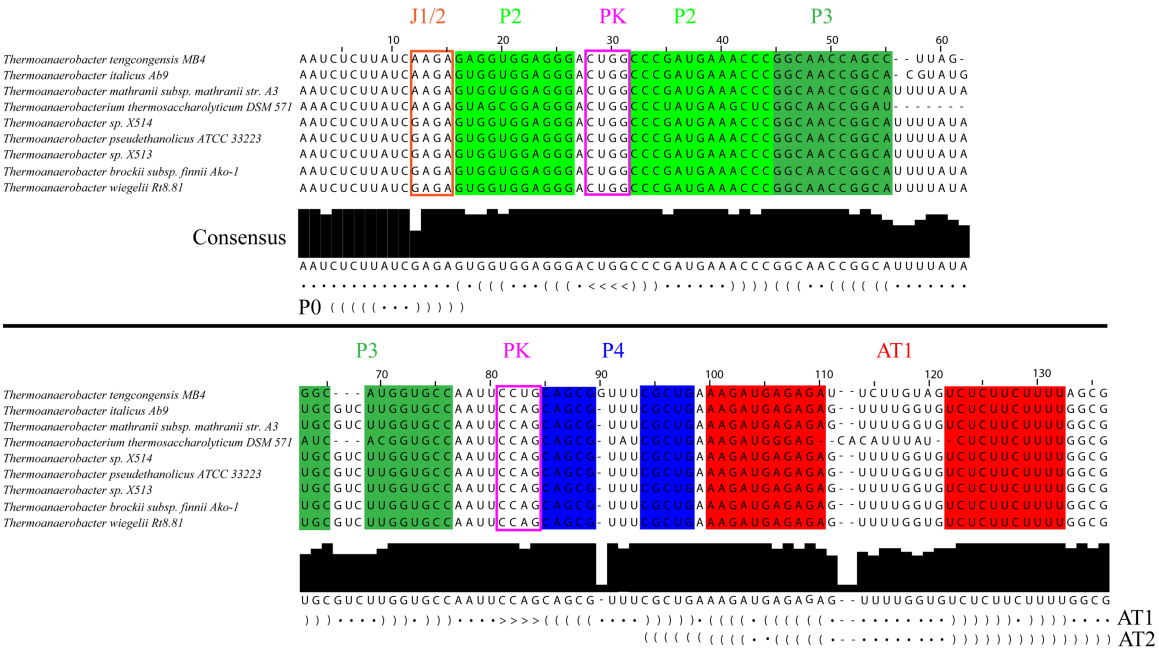

SI Figure 5. Sequence alignment of SAM-I riboswitch sequences that are upstream of the metF gene in several thermophilic anaerobic bacteria.

Helical regions are masked in color blocks and labeled according to the corresponding helix. The pseudoknot (PK) is boxed in pink, and J1/2 in orange. Alternative secondary structural elements (P0, AT2) are also shown in dot-bracket representation (as used in the Vienna package)[16] at corresponding regions.

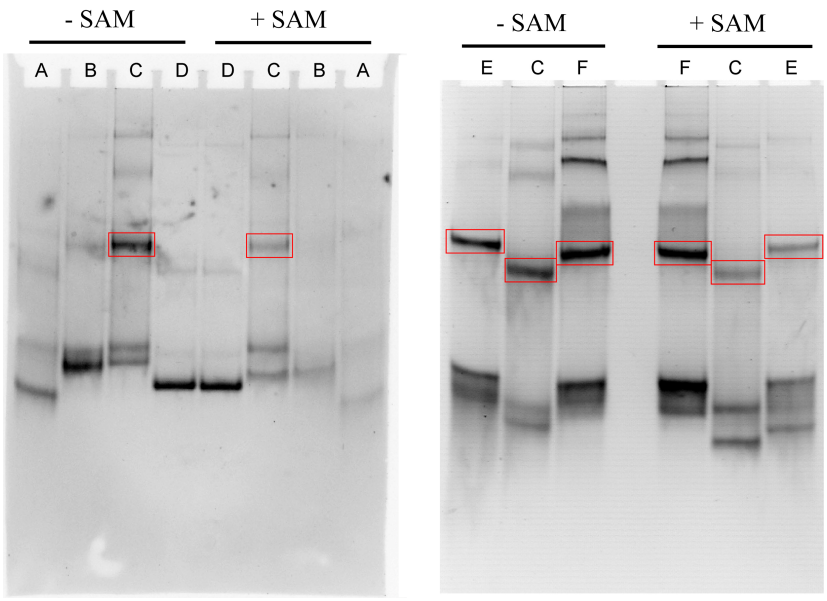

SI Figure 6. Native gel mobility of the *T.tengcongenesis metF* SAM-I riboswitch and mutants at different length of transcript.

RNA was folded in 1x TB (pH 8.3), 200 mM KCl, 10 mM $MgCl_2$, 20% Glycerol with or without 100 μM SAM. Sample A, WT aptamer (3' end at position 0 as labeled in the *T.tengcongesis* sequence in Fig. 1); sample B, WT AAT_AT1 (3' end at position 16); sample C, eP0 AT1 (mutant to destabilize the P1 helix and stabilize the proposed P0 helix, 3' end at position 16); sample D, 5'AUCP1_AT1 (WT AAT_AT1 with 5' end sequence before AUC nucleotides truncated); sample E, WT AAT_AT2 (3' end at position 25); sample F, eP0 AT2 (P0 mutant 3' end at position 25). A conformation state that has slow mobility and its population reduced in the presence of SAM is highlighted in the red rectangle box. All samples show increased mobility with added SAM for the fastest running band, except D. The remaining samples also seem to indicate an increase in the relative population within the fastest running band with added SAM, except F, which has been mutated to stabilize AT-forming conformation.

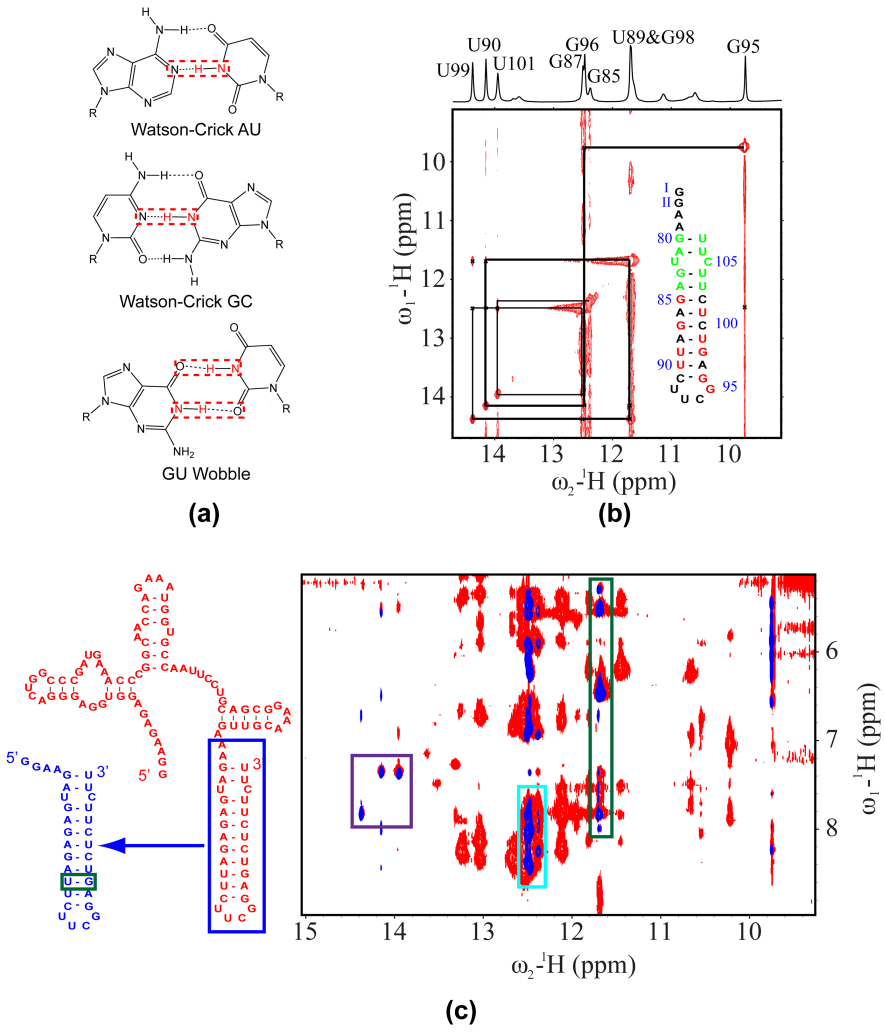

SI Figure 7. NMR spectra of RNA constructs isolated AT_U2 and GGAA_AT_U2.

(a) Schematic of Watson-Crick AU, Watson-Crick GC and wobble GU base pair. The imino proton that resonates in the 10-15 ppm region is highlighted in red. (b) Imino to imino proton region of a NOESY of isolated AT_U2 RNA (consisting of an AT1 helix RNA with two U residues truncated from the 3' end) at 15 °C in 10 mM KPhosphate, 10 mM KCl, 0.01 mM EDTA, pH=6.0 with a mixing time of 300 ms. The standard A-form resonance assignment walk in the stem region close to the UUCG tetraloop is indicated by a black line. Nucleotides with imino protons assigned are highlighted in red in the schematic. (c) Superposition of imino to aromatic/amino proton region between the 100 ms NOESY spectrum of a "ON" state conformer (GGAA_AT_U2, constrained from forming a P1 helix by 5' truncation) in 10 mM NaPhosphate, 10 mM NaCl, 0.01 mM EDTA, pH=6.0 at 15 °C and the 300 ms NOESY spectrum of isolated_AT_U2 in panel (a). Note that the U89:G98 base pairing (green box) is replaced by an AU pair in the P1 helix context in the schematic at left. Cross peaks corresponding to AU base pairs are highlighted in a purple box, and a subset of those associated with GC pairs is in a cyan box. All spectra in Figures 7 and 8 were acquired in 90% H_2O, 10 % D_2O. These spectra

confirm the presence of the AT1 helix in the larger construct and enable the assignment of corresponding imino resonances.

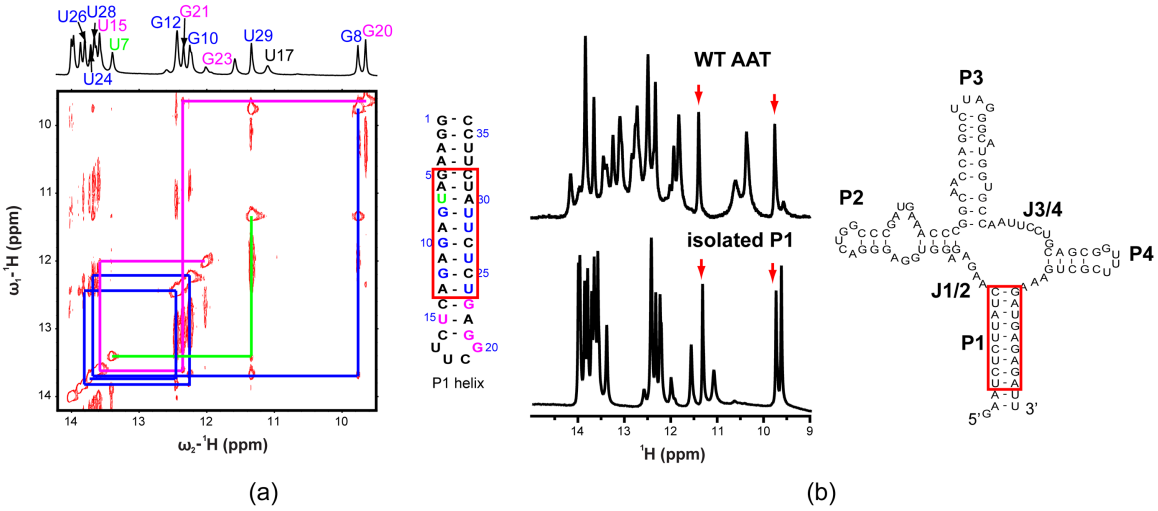

SI Figure 8. NMR spectra of isolated P1 helix and WT AAT RNA.

(a) Imino to imino proton region of a 250 ms NOESY of a model RNA stem loop containing a P1 helix sequence at 7 °C. Buffer: 20 mM NaPhosphate, pH=6.0. The sequence of the isolated P1 helix is shown at the right with a red rectangle box highlighting the region which matches that of the P1 helix in the large RNA construct. Residues with imino proton assigned are color coded by region. (b) Superposition of the 1D imino proton of WT AAT and isolated P1 helix. The sequence of WT AAT is shown at the right in secondary structure representation. The red arrows highlight the imino proton signals from the only GU base pair in the P1 helix. These spectra show the formation of the P1 helix within the larger construct and enable the assignment of corresponding imino resonances.

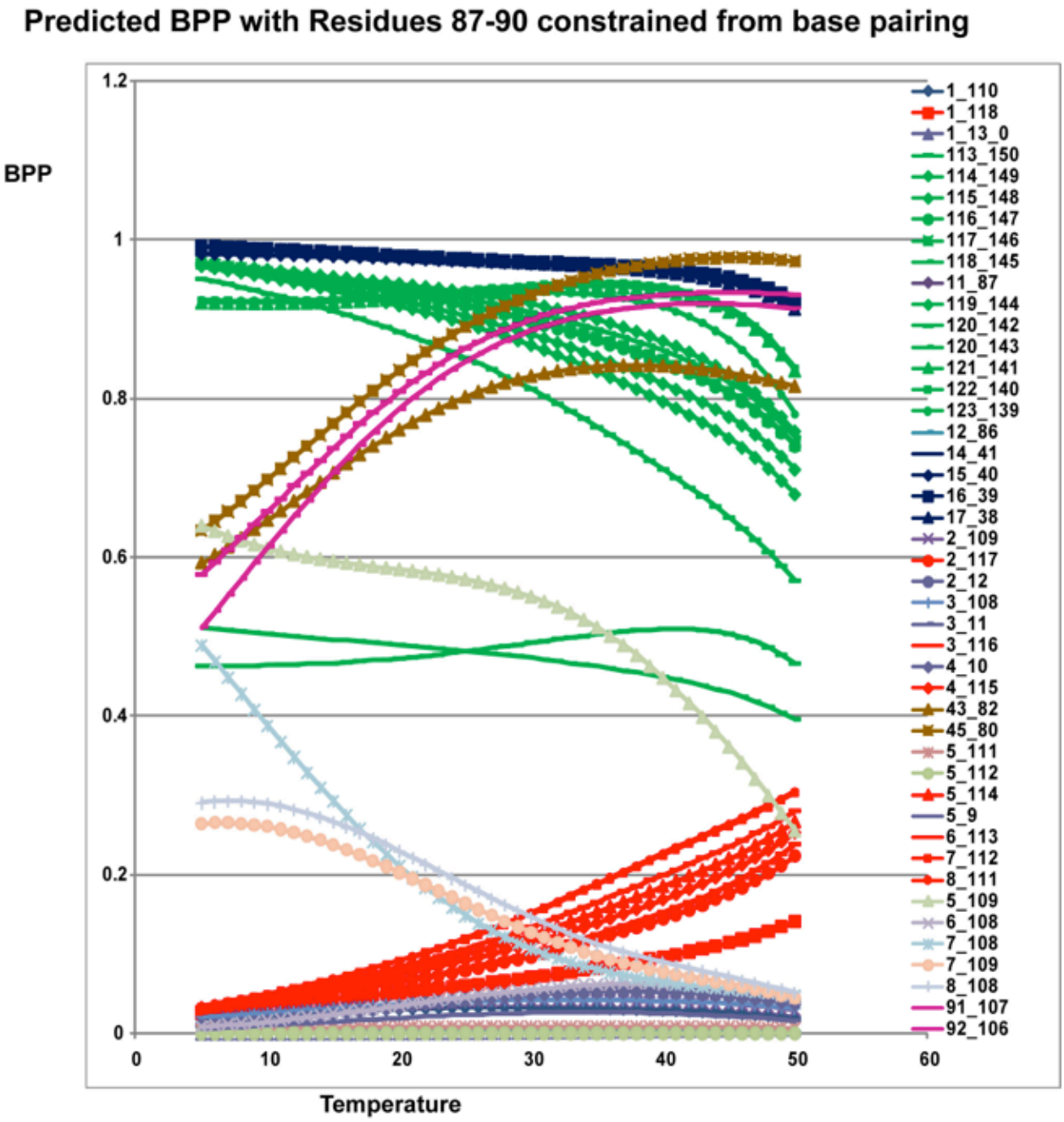

SI Figure 9. Prediction of selected BPPs for the *yitJ* SAM-I riboswitch sequence.

The transcript length used here is 151 nucleotides, as shown in Figure 5b in the main text, except that residues in J3/4 that participate in pseudoknot formation (87-90) are constrained from participating in base pairing. Base pairings are color coded as red for the P1 helix, blue for the P2 helix, brown for P3, magenta for P4, green for the AT helix, and gray for the P0 helix. Note that base pairs involving the 5' residues of the P1 helix pairing with residues in J3/4 (5-109, 7-108, and 7-109) are prominent at low temperature.

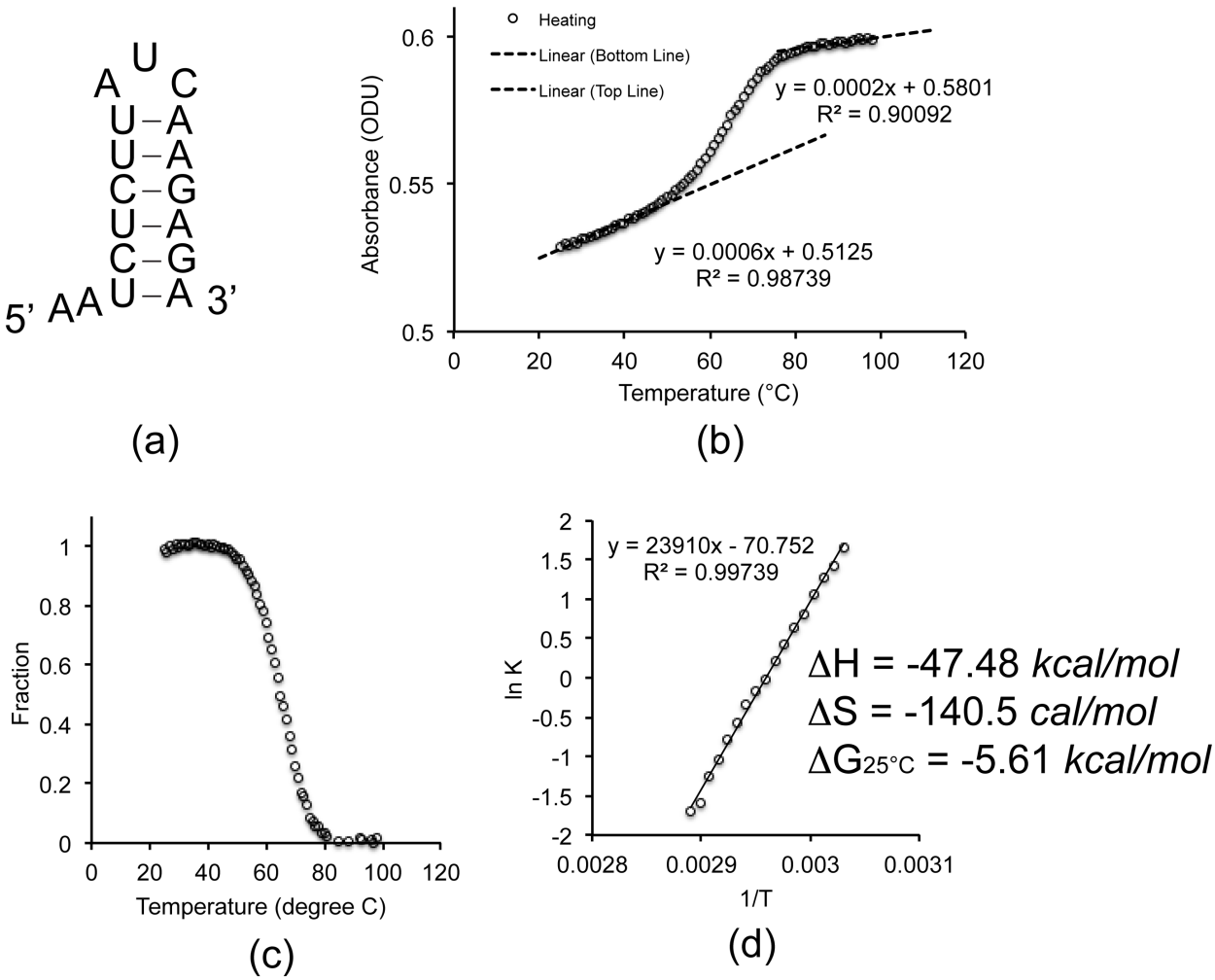

SI Figure 10. UV melting experiment of isolated *metF* SAM-I riboswitch P0 helix-forming segment.

(a) Sequence of the isolated P0 helix in secondary structure representation. (b) Melting profile of isolated P0 helix in buffer condition: 50 mM KPhos, 150 mM KCl, 0.02 mM EDTA, pH=7.5 (similar condition as the buffer used in fluorescence experiment except without Mg2+). (c) Normalization of the melting data. (d) Thermodynamic parameters by fitting lnK vs. 1/T.

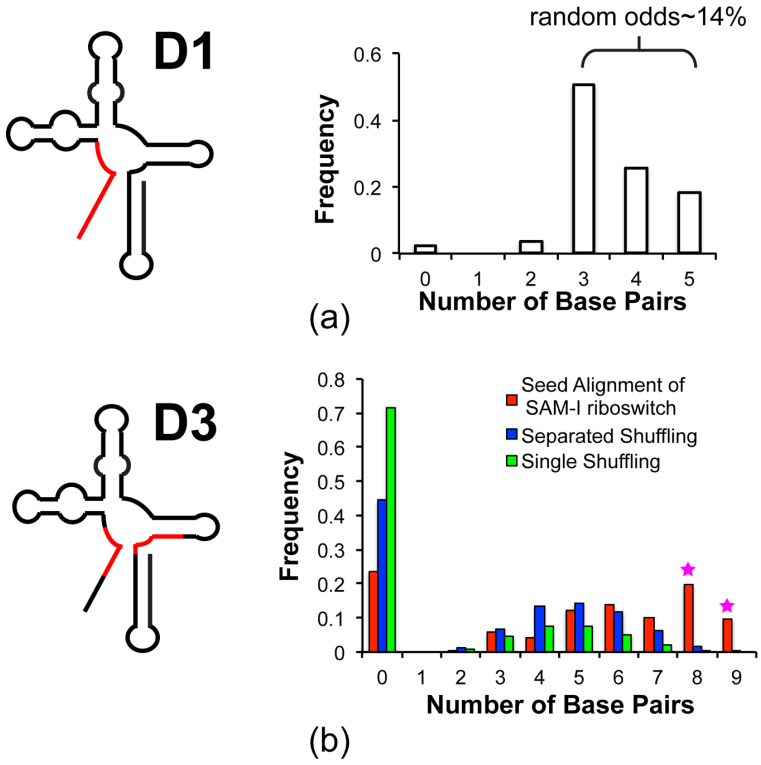

SI Figure 11. Sequence survey indicates high occurrence of potential D1 and D3 helix formation in SAM-I riboswitches.

(a) Survey on the number of possible consecutive base pairs for D1 (P0 helix) (defined in Figure 5a and in SI Figure 1c). The sequences were truncated based on the full sequence alignment of 2828 SAM-I riboswitches from Rfam 72. The region that is used in this sequence analysis is the red strand segment in the schematic on the left. The length of this region is 13 nt—5 upstream of the highly conserved 5'-AUC-3' segment in the P1 helix and 5 downstream. (b) Survey on the number of possible base pairs in the D3 helix (Figure 5a and SI Figure 1c). The SAM-I riboswitch sequences used here are from the seed alignment from Rfam 72. The distribution of possible base pairs between these two regions in the SAM-I riboswitch sequences are compared to that of 10,000 random sequences generated by shuffling. The shuffling is allowed for both intra-strand (separated shuffling) and inter-strand (single shuffling). The bimodal distribution implies that the D3 interaction has been selected for in a subset of SAM-I riboswitch sequences.

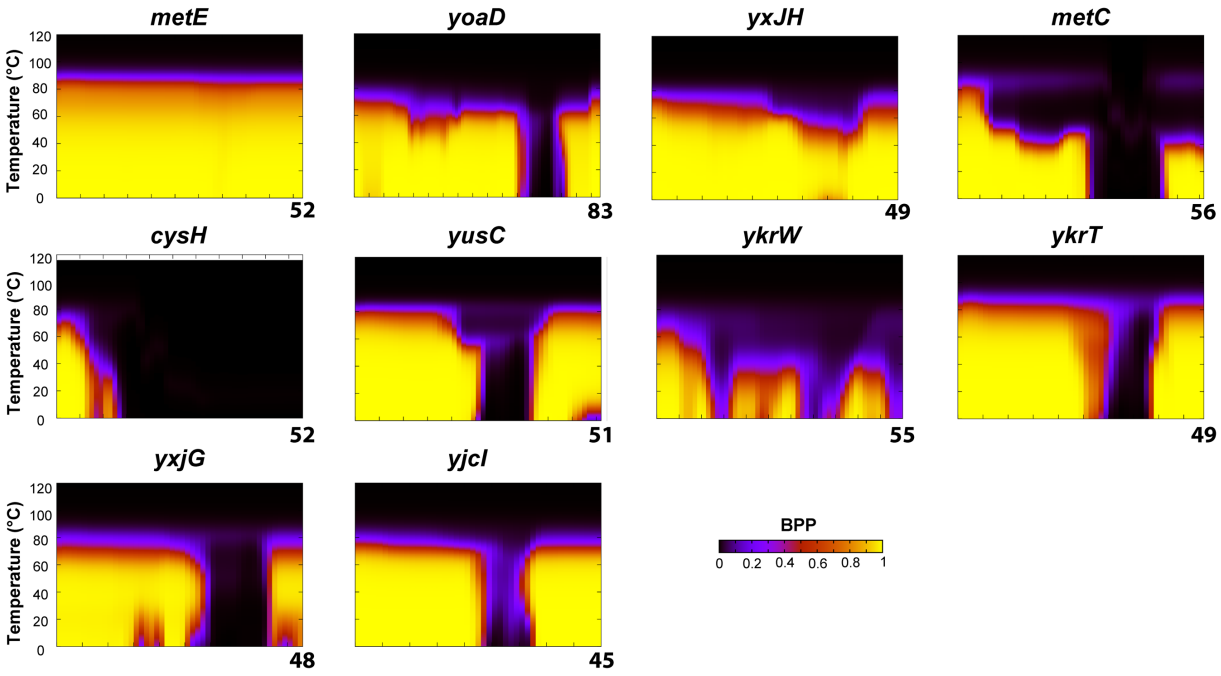

SI Figure 12. Closing base pair of the P1 helix-BPP calculations of other riboswitches in *B.subtilis*.

(a) Heat maps of *B. subtilis* SAM-I riboswitch sequences from reference [13] calculated and plotted as for Figure 1, except that here the nucleotide length on the horizontal axis is counted beginning from the terminus of the aptamer as position 0. Only the BPP of the base pair at the helical end close to the junction region is displayed here. A wide range of co-transcriptional folding patterns is predicted.

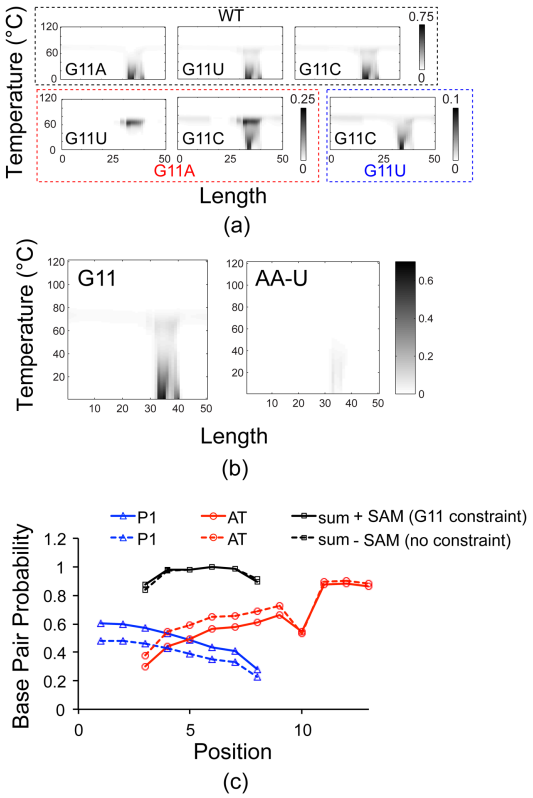

SI Figure 13. The contribution from G11 conformational heterogeneity to riboswitch functional folding.

(a) The difference in BPP (P1 helix base pair at position 1) between two RNA constructs. The reference RNA construct is the wild type sequence for the top panel, and is specified underneath the plot in the lower panels. For example, the panel labeled "G11A" and boxed in red shows the difference in P1 helix BPP for the G11U (left) or G11C (right) mutants and the P1 helix BPP for the G11A mutant. The color scale is on the right. The darker the dot the greater the enhancement of the BPP in the specified mutant RNA construct compared with the reference construct. (b) BPP calculation with constraints designed to mimic SAM binding. The difference between BPP (base pair at position 1 Fig.2) calculated with and without the specified constraints is plotted. Left: G11 unpaired, to mimic the effect of SAM contacting G11; Right: AA-U internal loop to mimic the effect of SAM replacing two As as potential pairing partners with U in P3 helix internal loop[3; 17]. (c) Comparison of BPPs for base pairs in the P1 and the AT helix at 37 °C with the constraint—G11 unpaired (solid line) and that without any constraint (dash). Within the region predicted to most readily favor AT helix formation, restricting G11 base pairing consistently increases BPP for P1 helix formation.

References

1. Shin, S. J., Wu, C.-w., Steinberg, H. & Talaat, A. M. (2006). Identification of Novel Virulence Determinants in Mycobacterium paratuberculosis by Screening a Library of Insertional Mutants. *Infect. Immun.* **74**, 3825-3833.
2. Heppell, B. & Lafontaine, D. A. (2008). Folding of the SAM aptamer is determined by the formation of a K-turn-dependent pseudoknot. *Biochemistry* **47**, 1490-1499.
3. Montange, R. K., Mondragón, E., van Tyne, D., Garst, A. D., Ceres, P. & Batey, R. T. (2010). Discrimination between closely related cellular metabolites by the SAM-I riboswitch. *Journal of Molecular Biology* **396**, 761-772.
4. Gilbert, S. D., Montange, R. K., Stoddard, C. D. & Batey, R. T. (2006). Structural studies of the purine and SAM binding riboswitches. *Cold Spring Harb Symp Quant Biol* **71**, 259-68.
5. Heppell, B., Blouin, S., Dussault, A.-M., Mulhbacher, J., Ennifar, E., Penedo, J. C. & Lafontaine, D. A. (2011). Molecular insights into the ligand-controlled organization of the SAM-I riboswitch. *Nat Chem Biol* **7**, 384-392.
6. Reuter, J. & Mathews, D. (2010). RNAstructure: software for RNA secondary structure prediction and analysis. *BMC Bioinformatics* **11**, 129.
7. Bellaousov, S. & Mathews, D. H. (2010). ProbKnot: Fast prediction of RNA secondary structure including pseudoknots. *RNA* **16**, 1870-1880.
8. Takamoto, K., Chance, M. R. & Brenowitz, M. (2004). Semi-automated, single-band peak-fitting analysis of hydroxyl radical nucleic acid footprint autoradiograms for the quantitative analysis of transitions. *Nucleic Acids Research* **32**, E119.
9. Das, R., Laederach, A., Pearlman, S. M., Herschlag, D. & Altman, R. B. (2005). SAFA: semi-automated footprinting analysis software for high-throughput quantification of nucleic acid footprinting experiments. *RNA* **11**, 344-54.
10. Hennelly, S. P. & Sanbonmatsu, K. Y. (2010). Tertiary contacts control switching of the SAM-I riboswitch. *Nucleic Acids Res*.
11. Winkler, W. C., Nahvi, A., Sudarsan, N., Barrick, J. E. & Breaker, R. R. (2003). An mRNA structure that controls gene expression by binding S-adenosylmethionine. *Nature Struct. Biology* **10**, 701-707.
12. McDaniel, B. A. M., Grundy, F. J., Artsimovitch, I. & Henkin, T. M. (2003). Transcription termination control of the S box system: Direct measurement of S-adenosylmethionine by the leader RNA. *Proceedings National Acadamy of Sciences, USA* **100**, 3083-3088.
13. Tomsic, J., McDaniel, B. A., Grundy, F. J. & Henkin, T. M. (2008). Natural variability in S-Adenosylmethionine (SAM)-dependent riboswitches: S-Box elements in *Bacillus subtilis* exhibit differential sensitivity to SAM in vivo and in vitro. *Journal of Bacteriology* **190**, 823-833.
14. Montange, R. K. & Batey, R. T. (2006). Structure of the S-adenosylmethionine riboswitch regulatory mRNA element. *Nature* **441**, 1172-1175.
15. Hennelly, S. P. & Sanbonmatsu, K. Y. (2011). Tertiary contacts control switching of the SAM-I riboswitch. *Nucleic Acids Research* **39**, 2416-2431.

16. Hofacker IL, Fontana W, Stadler PF, Bonhoeffer LS, Tacker M & Schuster P. (1994). Fast folding and comparison of RNA secondary structures (The Viennna Package). *Monatshefte fur Chemie (Chemical Monthly)* **125**, 167-188.
17. Stoddard, C. D., Montange, R. K., Hennelly, S. P., Rambo, R. P., Sanbonmatsu, K. Y. & Batey, R. T. (2010). Free state conformational sampling of the SAM-I riboswitch aptamer domain. *Structure* **18**, 787-797.